



## Rapid Prototyping Journal

Impedance-based non-destructive evaluation of additively manufactured parts  
Mohammad I. Albakri, Logan D. Sturm, Christopher B. Williams, Pablo A. Tarazaga,

### Article information:

To cite this document:

Mohammad I. Albakri, Logan D. Sturm, Christopher B. Williams, Pablo A. Tarazaga, (2017) "Impedance-based non-destructive evaluation of additively manufactured parts", Rapid Prototyping Journal, Vol. 23 Issue: 3, pp.589-601, <https://doi.org/10.1108/RPJ-03-2016-0046>

Permanent link to this document:

<https://doi.org/10.1108/RPJ-03-2016-0046>

Downloaded on: 03 September 2017, At: 07:45 (PT)

References: this document contains references to 22 other documents.

To copy this document: [permissions@emeraldinsight.com](mailto:permissions@emeraldinsight.com)

The fulltext of this document has been downloaded 114 times since 2017\*

### Users who downloaded this article also downloaded:

(2017), "Current state and potential of additive – hybrid manufacturing for metal parts", Rapid Prototyping Journal, Vol. 23 Iss 3 pp. 577-588 <<https://doi.org/10.1108/RPJ-04-2016-0065>>

(2017), "Pre and post processing techniques to improve surface characteristics of FDM parts: a state of art review and future applications", Rapid Prototyping Journal, Vol. 23 Iss 3 pp. 495-513 <<https://doi.org/10.1108/RPJ-05-2015-0059>>



Access to this document was granted through an Emerald subscription provided by emerald-srm:234115 []

### For Authors

If you would like to write for this, or any other Emerald publication, then please use our Emerald for Authors service information about how to choose which publication to write for and submission guidelines are available for all. Please visit [www.emeraldinsight.com/authors](http://www.emeraldinsight.com/authors) for more information.

### About Emerald [www.emeraldinsight.com](http://www.emeraldinsight.com)

Emerald is a global publisher linking research and practice to the benefit of society. The company manages a portfolio of more than 290 journals and over 2,350 books and book series volumes, as well as providing an extensive range of online products and additional customer resources and services.

Emerald is both COUNTER 4 and TRANSFER compliant. The organization is a partner of the Committee on Publication Ethics (COPE) and also works with Portico and the LOCKSS initiative for digital archive preservation.

\*Related content and download information correct at time of download.

# Impedance-based non-destructive evaluation of additively manufactured parts

*Mohammad I. Albakri*

Vibrations, Adaptive Structures, and Testing Laboratory, Department of Mechanical Engineering,  
Virginia Polytechnic Institute and State University, Blacksburg, Virginia, USA

*Logan D. Sturm and Christopher B. Williams*

Design, Research, and Education for Additive Manufacturing Systems Laboratory, Department of Mechanical Engineering,  
Virginia Polytechnic Institute and State University, Blacksburg, Virginia, USA, and

*Pablo A. Tarazaga*

Vibrations, Adaptive Structures, and Testing Laboratory, Department of Mechanical Engineering,  
Virginia Polytechnic Institute and State University, Blacksburg, Virginia, USA

## Abstract

**Purpose** – This work proposes the utilization of electromechanical impedance measurements as a means of non-destructive evaluation (NDE) for additive manufacturing (AM). The effectiveness and sensitivity of the technique for a variety of defect types commonly encountered in AM are investigated.

**Design/methodology/approach** – To evaluate the feasibility of impedance-based NDE for AM, the authors first designed and fabricated a suite of test specimens with build errors typical of AM processes, including dimensional inaccuracies, positional inaccuracies and internal porosity. Two polymer AM processes were investigated in this work: material jetting and extrusion. An impedance-based analysis was then conducted on all parts and utilized, in a supervised learning context, for identifying defective parts.

**Findings** – The newly proposed impedance-based NDE technique has been proven to be an effective solution for detecting several types of print defects. Specifically, it was shown that the technique is capable of detecting print defects resulting in mass change (as small as 1 per cent) and in feature displacement (as small as 1 mm) in both extruded nylon parts and jetted VeroWhitePlus parts. Internal porosity defects were also found to be detectable; however, the impact of this defect type on the measured impedance was not as profound as that of dimensional and positional inaccuracies.

**Originality/value** – Compared to currently available NDE techniques, the newly proposed impedance-based NDE is a functional-based technique with the advantages of being cost-effective, sensitive and suitable for inspecting AM parts of complex geometry and deeply embedded flaws. This technique has the potential to bridge the existing gaps in current NDE practices, hence paving the road for a wider adoption of AM to produce mission-critical parts.

**Keywords** Additive manufacturing, Electromechanical impedance, Non-destructive evaluation, Printing defects

**Paper type** Research paper

## 1. Introduction

### 1.1 Challenges of quality control for additively manufactured parts

As additive manufacturing (AM) technologies and materials continue to mature, there has been a sudden and significant increase in the number of end-use products fabricated via AM. AM technologies' layer-wise approach to fabrication provides designers the opportunities to realize products featuring complex geometries that can be tailored to simultaneously meet several design objectives and functionalities. These advances have been observed predominately in the aerospace industry where highly valued, highly engineered and

customized products are produced in low volumes, which fit well with current economic justifications for AM implementation. Some of the notable applications of AM technologies to fabricate end-use aerospace products include both printed metals (e.g. GE Aviation's LEAP 56 fuel nozzle [Figure 1(a)] and SpaceX's SuperDraco combustion chamber for the Dragon V2 rocket engine [Figure 1(b)]) and polymers (e.g. FAA-approved ULTEM 9085 aircraft air duct created by Stratasys and Orbis [Figure 1(c)]).

While efforts in using AM technology to produce end-use parts are rapidly advancing, research and development of quality control (QC) techniques to validate these parts is

The current issue and full text archive of this journal is available on Emerald Insight at: [www.emeraldinsight.com/1355-2546.htm](http://www.emeraldinsight.com/1355-2546.htm)



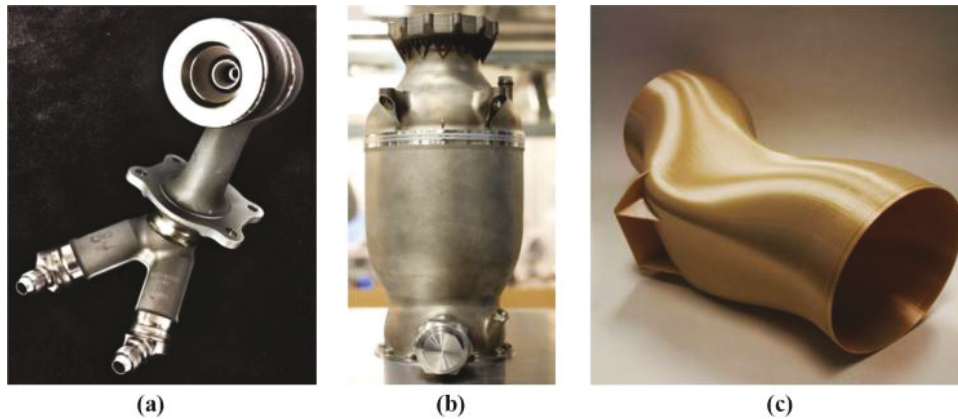
Rapid Prototyping Journal  
23/3 (2017) 589–601  
© Emerald Publishing Limited [ISSN 1355-2546]  
[DOI 10.1108/RPJ-03-2016-0046]

This material is based upon work supported by the National Science Foundation under Grant No. #1446804. Any opinions, findings and conclusions or recommendations expressed in this material are those of the author(s) and do not necessarily reflect the views of the National Science Foundation.

Received 21 March 2016

Revised 22 June 2016

Accepted 25 June 2016

**Figure 1** Example applications of AM to fabricate end-use aerospace components

**Notes:** (a) GE fuel nozzle; (b) SpaceX combustion chamber; (c) Stratasys/Orbis' conformal air duct (Stratasys, 2015)

lacking. Perhaps ironically, the challenges in qualification of AM stem from the complexity that AM offers to designers. Complex geometries that contain inaccessible features (e.g. internal channels) cannot be quickly measured using conventional metrology techniques. This, along with the frequent occurrence of deeply embedded flaws (e.g. internal porosity and cracks) in direct-metal powder-bed fusion processes, requires non-destructive evaluation (NDE) techniques for part qualification.

However, current NDE techniques are not readily suitable for analysis of AM parts. Dimensional measurement techniques such as coordinate measuring machines (CMM) and structured light (SL) scanning require access to all surfaces of the part, which is not always certain given the design freedom offered by AM. While eddy current testing (ECT) and ultrasonic testing (UT) techniques can be used to detect internal porosity, their application to AM parts is limited as they must have access to all surfaces (because of their limited surface penetration) and they are sensitive to surface roughness. Penetrant testing and magnetic particle testing techniques are less geometry-sensitive; however, they could not be used for assessing parts with intricate internal features.

Computed tomography (CT) is currently the NDE technique most often used with AM, as it can readily inspect the entirety of the part regardless of its geometry and internal structure. CT has been demonstrated by NASA to detect deep/embedded defects, interrogate inaccessible features and characterize and qualify as-manufactured AM parts (Waller *et al.*, 2014). Improvements have also been made in the ability to classify and quantify printing defects instead of simple qualitative measurements (Plessis *et al.*, 2015). However, there are a number of limitations to the use of CT as a means for inspecting AM parts. It is costly and time-intensive. It is not able to reliably detect cracks that are oriented perpendicular to the X-ray beam. There also exists a tradeoff in penetration depth and the resolution of the inspection, which could result in a failure of identifying deeply embedded micro-porosity. Furthermore, larger parts are pushing the physical limits of the existing CT systems.

## 1.2 Non-destructive evaluation for additive manufacturing

In their *Measurement Science Roadmap for metal-based Additive Manufacturing*, NIST states that “Existing NDE techniques are not optimized for AM processes, materials or parts. Techniques are lacking for in-situ NDI, and post-process AM part inspection”. The authors suggest that an ideal post-process NDE technique for AM would have the following attributes:

- Cost-effective.
- Able to be conducted quickly.
- Able to evaluate parts irrespective of geometry, surface and material. In other words, the technique would be able to analyze inaccessible features, large parts, fine features, rough surface finish, etc.
- Able to detect typical AM build errors including feature location deviation, feature size (part mass deviation) and deeply embedded flaws.

In addition to the aforementioned requirements, the authors suggest that an ideal NDE technique would also be free of cyber-physical vulnerabilities. As discussed in their previous work (Sturm *et al.*, 2014), the authors suggest several cyber-physical security vulnerabilities in AM and QC because of the reliance on digital files throughout the process chain (CAD files, STL files, toolpath files, AM machine firmware and even the output of the metrology system), which can be easily altered by an attacker. Thus, an ideal NDE technique would be separate from the system and part data, and instead treated as a second-channel measurement of the AM process's functionality.

In this regard, such an ideal AM NDE technique would resemble existing functional testing schema for evaluating printed circuit boards (PCBs). When PCBs are qualified, one does not test the connectivity of every solder point on the board or the tolerance of the part placement. Instead, one tests the functionality of the PCB by placing an input voltage into the board and measuring its functional response. This type of in-line go or no-go decision-making is ideal for a post-process NDE technique as it is cost-effective, quick and cyber-secure.

1.3 Research goal

The lack of reliable means for verifying the quality of printed parts is a significant barrier to further industrial adoption of AM technologies. Without a means of performing part validation and certification, it is not possible to expand the use of AM for the fabrication of mission-critical parts. As such, the need for NDE techniques that are optimized for AM has been identified as a research area of critical importance by several organizations such as NIST (2013), NASA (2014) and the ASTM F-42 committee (2017). Because of the established deficiencies of existing NDE techniques, NIST’s roadmap action plan suggests that the community conducts research and development for new post-process NDE techniques that are optimized for AM.

To address this research gap, the authors propose to use electromechanical impedance measurements as a means to detect and identify AM defects. Impedance measurements have laid the foundation for the impedance-based structural health monitoring (SHM) technique, which has been successfully applied to assess the integrity of a wide spectrum of civil structures and mechanical components. It is hypothesized that such quick, non-intrusive measurements will allow observation of parts deviations when compared to measurements of equivalent defect-free parts. A detailed overview of impedance-based SHM and its extension to NDE of AM parts is provided in Section 2.

The overall goal of this paper is to show and assess the feasibility of using electromechanical impedance measurements for NDE of AM parts. This research is guided by two primary research questions:

RQ1. “What type of defects can impedance-based NDE detect?”

RQ2. “What defect sizes can it detect?”

To answer these questions, the authors designed and printed a series of test specimens which contain build errors typical of AM processes (as described in Section 3.1). Impedance measurements were conducted and compared against a pair of defect-free parts (Section 3.2-3.3). Results from this comparison are presented and analyzed in Section 4. Closure and future work are presented in Section 5.

2. Electromechanical impedance for SHM and NDE

The fundamental basis of vibration-based SHM and damage identification techniques is that the presence of damage will alter the mass, stiffness and damping characteristics of the structure, which in turn reflect on its measured dynamic response. Among the different SHM techniques, impedance-based SHM has emerged as a promising, non-intrusive, cost-effective and highly sensitive solution for real-time damage assessment (Park et al., 2003). This technique utilizes piezoelectric materials, lead zirconate titanate (PZT) wafers in particular, as collocated sensors and actuators to simultaneously excite the structure and measure its response (Liang et al., 1994; Giurgiutiu and Zagrai, 2000). Making use of the coupled electromechanical behavior of piezoelectric materials, the problem of measuring the mechanical impedance of the host

structure is significantly simplified, and it is directly related to the easily measurable electrical impedance of the piezoelectric transducer. Therefore, variations in the host structure due to printing defects are reflected on the electrical impedance of the piezoelectric transducers, and thus, can be detected and identified (Park et al., 2000a; Albakri and Tarazaga, 2016; Albakri et al., 2015).

Figure 2 shows a schematic of a piezoelectric transducer attached to a printed part, which is represented by an equivalent spring, mass and damper system. Assuming linear piezoelectricity, the constitutive equations of piezoelectric materials operating in 31 mode can be expressed as (Leo, 2007).

$$\begin{aligned} \epsilon_{11} &= s_{11}^E \sigma_{11} + d_{13} E_3 \\ D_3 &= (d^T)_{31} \sigma_{11} + \epsilon_{33}^E E_3, \end{aligned} \tag{1}$$

where  $\epsilon_{11}$  is the Green strain tensor component in the 1-direction,  $\sigma_{11}$  is the corresponding component of the work-conjugate stress tensor,  $D_3$  is the electric displacement in the 3-direction,  $E_3$  is the electric field in the 3-direction,  $d_{13}$  is the piezoelectric coupling coefficient,  $s_{11}^E$  is the complex mechanical compliance of the material measured at zero electric field. For the simplified One-dimensional, plane-stress problem at hand,  $s_{11}^E$  reduces to the inverse of the Young’s modulus of elasticity of the piezoelectric material.  $\epsilon_{33}^E$  is the complex permittivity measured at zero stress.

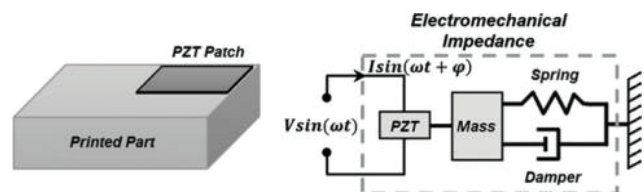
Because of the coupled electromechanical behavior of piezoelectric materials, the electrical impedance of the piezoelectric transducer is directly related to the mechanical impedance of the host structure,  $Z_{st}$ , as follows (Park et al., 2003)

$$Z(\omega) = \left[ i\omega \frac{bl}{h} \left( \frac{d_{13}^2}{s_{11}^E} \left( \frac{\tan(kl)}{kl} \left( \frac{Z_{pzt}}{Z_{pzt} + Z_{st}} \right) - 1 \right) + \epsilon_{33}^E \right) \right]^{-1}, \tag{2}$$

where  $Z_{pzt} = -iblh(s_{11}^E \omega \tan(kl)/kl)^{-1}$  is the piezoelectric transducer short-circuit impedance,  $k = \omega \sqrt{\rho s_{11}^E}$  is the wave number,  $\rho$  is the density of the piezoelectric material, and  $b$ ,  $h$  and  $2l$  are the piezoelectric patch width, thickness and length, respectively.

Being a vibration-based damage identification technique, the sensitivity of impedance-based SHM, along with the underlying electromechanical impedance measurements, is dependent on the frequency range at which the structure is interrogated. It has been shown that the wavelength of the excitation signal has to be smaller than the characteristic length of the defect for it to be successfully detected (Nokes and Cloud, 1993). Therefore, for enhanced sensitivity, impedance-based SHM is carried out at high frequencies.

Figure 2 A piezoelectric transducer attached to a mechanical structure represented by a spring-mass-damper system



Peairs *et al.* (2007) studied the possibility of preselecting preferred frequency ranges based on the free response of the piezoelectric transducers. They concluded that the characteristics of both the piezoelectric transducer and the host structure determine this optimal frequency range.

Electromechanical impedance measurements have been successfully applied to monitor the health of numerous civil, aerospace and mechanical components and structures. Park *et al.* (2000b) successfully implemented this technique for real-time damage detection in reinforced concrete walls, a bridge section and a pipe joint. Several other studies presented the successful utilization of electromechanical impedance measurements for detecting structural defects in a laboratory environment and under real operating conditions (Wang and Zou, 2013; Annamdas and Radhika, 2013; Zagrai *et al.*, 2010; Annamdas and Soh, 2010).

The authors hypothesize that electromechanical impedance measurements are especially relevant and appropriate for the inspection of AM parts, as it fits many of the needs identified in Section 1.2. The technique is cost-effective (i.e. no radiation source is needed), time-efficient (i.e. a full sweep across all frequencies of interest can be completed in seconds) and suitable for autonomous applications. When carried out at high frequency, electromechanical impedance measurements can be used to detect internal defects throughout the part without the need for accessing all points on the part's surface, and thus it is applicable for inspecting parts with intricate features.

### 3. Experimental methods

#### 3.1 Test specimen design and fabrication

To evaluate the effectiveness of electromechanical impedance measurements as a means of inspecting AM parts, the authors sought to design test parts that can replicate common types of defects occurring in parts fabricated using AM. The authors identified three types of generalized build errors common in all AM technologies:

- 1 *Dimensional inaccuracies*: These errors, in which the finished part has an incorrect final mass, can occur when either too much or too little material is deposited, fused or cured. This can occur if the machine is not properly configured or calibrated; e.g., the feed rate of an extrusion nozzle is too high, the laser power is too high, the droplet saturation level is too high, etc. This error can also occur due to machine failure; e.g., a misfire of a jetting nozzle, a clogged extrusion nozzle, poorly formed powder bed layer, etc. While the exact cause of excess or lack of material will vary process to process, the resulting error can occur across all AM processes.
- 2 *Positional inaccuracies*: These types of errors, in which the final part has the correct final mass but the deposited/formed mass is not accurately positioned, can be caused by improper machine calibration or machine error. This can occur if the stages' motors are not properly zeroed, there is an error in the toolpath file, the part warps during or after the build, etc.
- 3 *Internal porosity*: This error type refers to gaps or voids that are formed in the internal structure of a part during its build. This can occur because of process errors that result in a reduced melt pool size, incorrect tool path file or even

intentionally caused by a cyber-physical attack (Sturm *et al.*, 2014). This type of defects is unique to AM systems when compared to traditional subtractive manufacturing techniques. It differs from the aforementioned build errors, as it represents a loss of model material that is completely enclosed inside the part (thus preventing direct measurements with devices such as calipers). This error is difficult to detect not only because it is within the part structure but also because, depending on the nature of the AM process in question, this void may often be filled with unhardened model material or supporting material. The presence of this support material may result in the void having little to no effect on the mass of the part while significantly reducing its strength.

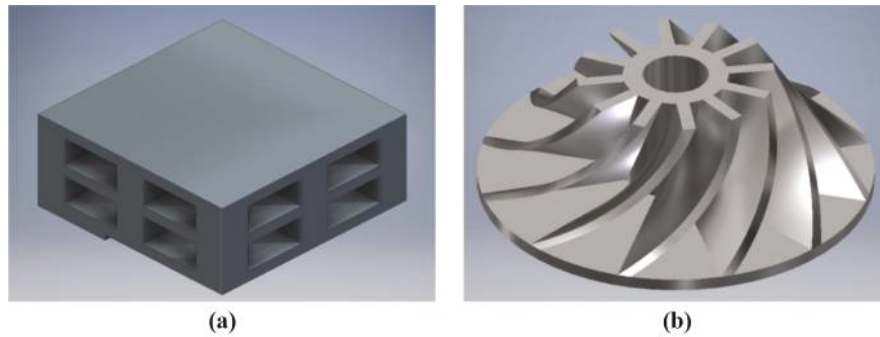
To assess the ability of impedance-based NDE to detect each of the aforementioned build errors, two test parts have been designed: a two-layer trussed structure and an impeller, as shown in Figure 3. The first part, which measures  $35 \times 35 \times 16 \text{ mm}^3$ , represents a truss topology consisting of nine pillars and two layers. The part is designed to allow for a systematic analysis of the technique's capabilities where defect type and overall size can be easily varied. This enables the researchers to identify the minimum defect size that can be detected. Multiple defect types can also be combined, enabling the examination of the effects of their interaction. The impeller, on the other hand, consists of a single base, 45 mm in diameter, and 12 fins evenly distributed around a 15-mm-high center pillar. Both parts include a small 1-mm-tall feature on the bottom surface, which is used to quickly and consistently guide sensor placement across all specimens.

Three sets of test specimens were fabricated by two different AM polymer processes: material jetting and extrusion. These processes were chosen, as they are commonly used AM systems representing two different structure types. Material jetting yields parts with high resolution and low internal porosity, while parts manufactured with material extrusion have coarser resolution with naturally occurring gaps between extruded lines of material. In more detail, specimens were fabricated in VeroWhitePlus (a stiff acrylate photopolymer) on a Stratasys Connex 350 multi-material jetting AM system and in nylon (a robust, engineering semi-crystalline thermoplastic) on a Stratasys Fortus 400 mc. The resulting test sets are as follows:

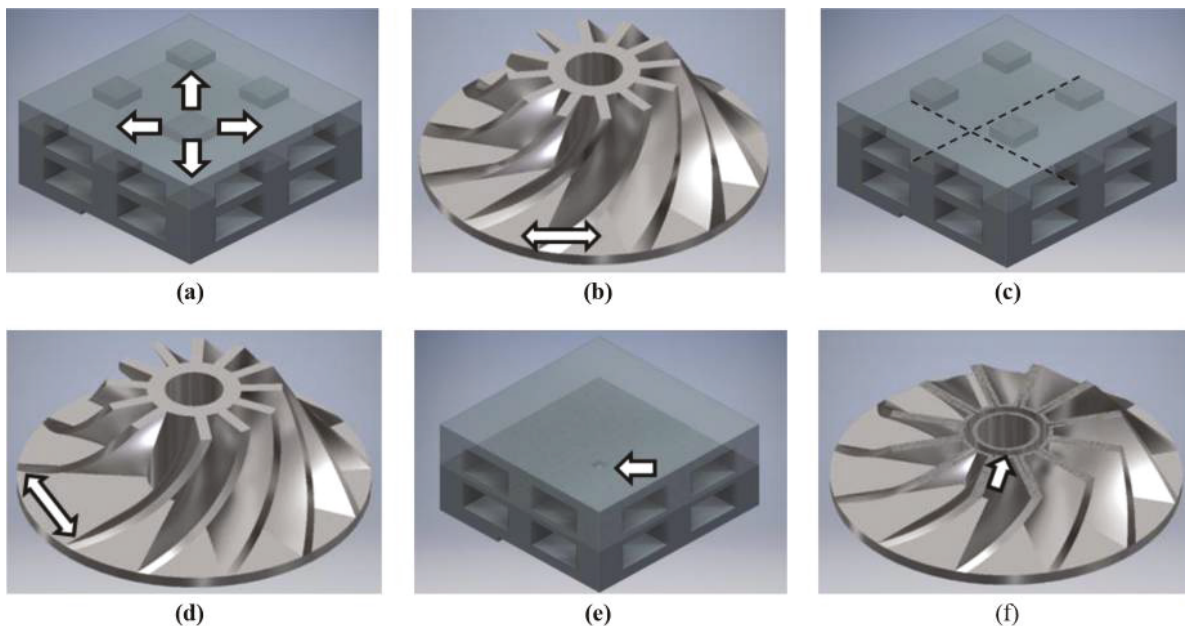
- *Test Set 1*: Trussed-structure specimens fabricated in VeroWhitePlus.
- *Test Set 2*: Trussed-structure specimens fabricated in nylon.
- *Test Set 3*: Impeller specimens fabricated in VeroWhitePlus.

Each test set consists of two unmodified, defect-free control parts, which are used to establish baseline responses, and additional six test parts featuring different build defect types as follows:

- 1 *Dimensional inaccuracy build defects*: This build defect is introduced by widening the center pillar of specimens in Test Set 1 and Test Set 2 [Figure 4(a)], resulting in a 1 and 5 per cent total mass increase. For Test Set 3, specimens with 5 per cent total mass increase were made by widening the base of the fins [Figure 4(b)].
- 2 *Positional inaccuracy build defects*: This defect type is introduced by moving the center pillar 1 mm diagonally

**Figure 3** Test parts designed to evaluate the capabilities of impedance-based NDE

**Notes:** (a) A trussed structure consisting of nine pillars and two layers; (b) a 12-fin impeller. The bottom features are used to guide sensor placement

**Figure 4** Tested defects

**Notes:** (a) 1 per cent mass increase of the part by widening the center pillar; (b) 5 per cent mass increase of the part by widening the base of the fins; (c) displacement of the center pillar by 1 mm; (d) 20-degree offset of fins' starting location; (e) 8-mm<sup>3</sup> void placed in the center pillar; (f) hollow center pillar

away from the sensor in a specimen in Test Sets 1 [Figure 4(c)], an upper surface warp in a specimen in Test Set 2 and a 20-degree offset of fins starting location in specimens in Test Sets 3 [Figure 4(d)].

- 3 *Internal porosity build defects:* This build defect is represented by introducing 1- and 8-mm<sup>3</sup> voids in the center and corner pillars of a number of specimens in Test Set 1, a 27-mm<sup>3</sup> void in the center pillar of a specimen in Test Set 2 [Figure 4(e)] and by a hollow center pillar in specimens in Test Sets 3 [Figure 4(f)]. Except for Test Set 2, all voids are completely filled with support material, resulting in a minimal change in parts' mass.

The defects in these specimens were chosen as they allow the evaluation of the proposed technique's ability to detect all

build errors and its sensitivity to defect size and location relative to the piezoelectric transducer.

### 3.2 Electromechanical impedance measurements

Once test specimens were printed, piezoelectric transducers were bonded to each of them guided by a small 1-mm-tall feature on their bottom surface. For each specimen set, all piezoelectric patches were diced out of the same piezoelectric wafer, and to the exact same dimensions so as to minimize uncertainties introduced by piezoelectric patches geometric and material characteristics. For Test Set 1, piezoelectric patches of 12.5 × 12.5 mm<sup>2</sup> were used, while 9.5 × 19 mm<sup>2</sup> patches were used for Test Sets 2 and 3. Superglue was used to bond the piezoelectric patches to the test specimens.

Figure 5(a)-(c) shows the test specimens of each test set with piezoelectric transducers bonded to them.

For each test specimen, impedance signature was measured using KEYSIGHT E4990A impedance analyzer. The frequency ranges selected for this study are 4-9 kHz for the nylon parts and 4-20 kHz for the VeroWhitePlus parts. These frequency ranges were selected such that the consistency of the impedance signatures corresponding to the defect-free control parts is maximized. It has been reported that, for metallic and composite structures, the frequency range over which the impedance signature is analyzed has a significant effect on the technique's sensitivity (Peairs *et al.*, 2007). The issue of optimal frequency range selection is still an active area of research and will be investigated in a later study. For both specimen sets, the frequency sweep was performed with a 10-Hz resolution. The impedance analyzer excites the piezoelectric transducers with a 1-V peak-to-peak sinusoidal signal and allows the structure to settle before measuring its response. To minimize the effects of noise contamination, eight measurements were averaged at each frequency step. Figure 5(d) shows one of the test specimens connected to the impedance analyzer during impedance measurement.

### 3.3 Damage detection and measurement analysis

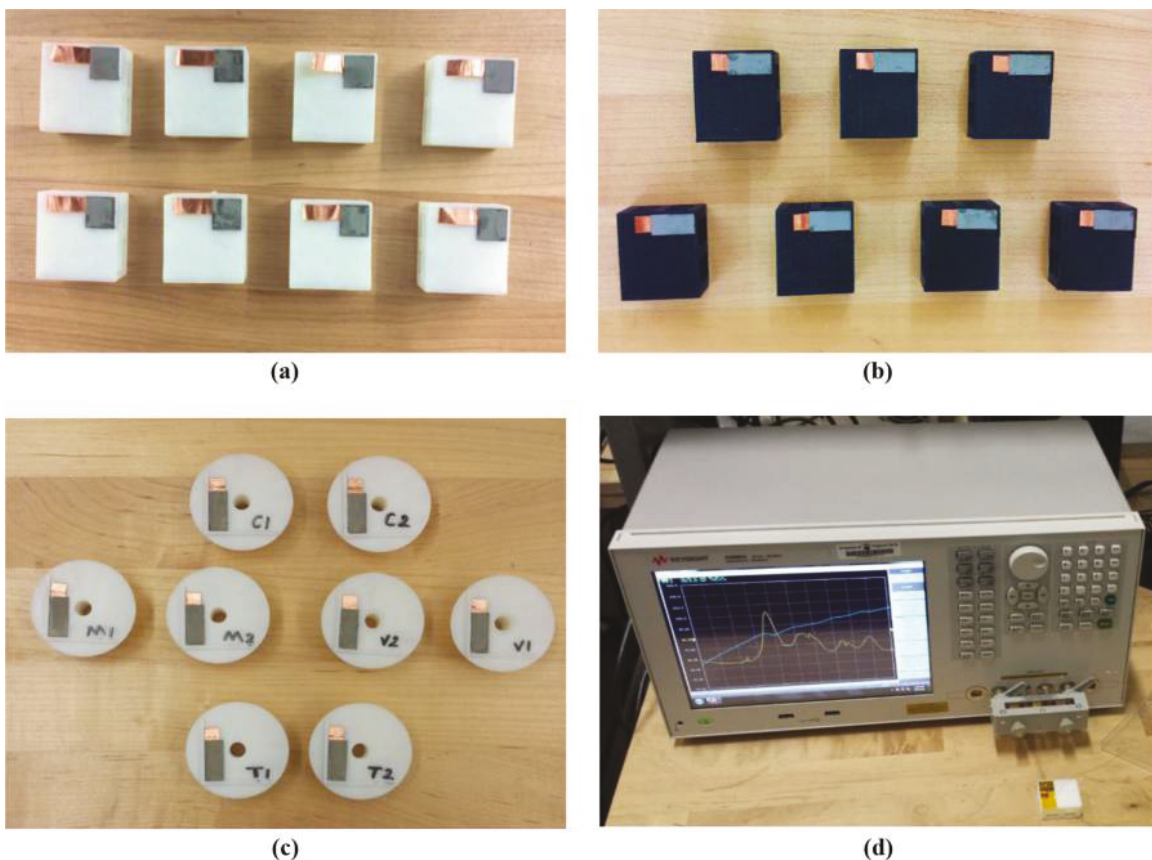
Impedance-based damage identification can be used in either supervised or unsupervised learning approaches. In unsupervised learning, the analysis technique can be

applied to an unknown set of parts and the damaged part(s) can be identified by analyzing the differences across all response signals. Alternatively, in a supervised learning approach, the impedance signatures of the parts being tested are compared to a baseline signature from a known defect-free part.

In this study, the authors situated the analysis in a supervised learning context. For each set of test specimens, two parts are known to be defect-free, as discussed in Section 3.1. These parts are used to establish a baseline signature to which all other parts are compared. The impedance signature baseline is obtained by averaging the impedance signatures of the two defect-free control parts. Only the real part of the measured impedance is considered in this study, as it is known to be more sensitive to the mechanical characteristics of the structure (Park *et al.*, 2003). The presence of printing defects in the other fabricated specimens changes the mechanical impedance of the part, which, in turn, is reflected on the measured impedance signatures. Therefore, changes in one part's impedance signature compared to the baseline signature can be used as an indicator of printing defects. To compensate for inconsistency in connectors' resistivity, as a result of soldering and wire length variations, all impedance signatures are shifted vertically such that their average value, excluding impedance peaks, match.

To quantify the variations in the impedance signature associated with each defect, two damage metrics are

**Figure 5** (a) Test Set 1, VeroWhitePlus trussed specimens; (b) Test Set 2, nylon trussed specimens; (c) Test Set 3, VeroWhitePlus impeller specimens; and (d) KEYSIGHT E4990A impedance analyzer measuring the impedance signature of one specimen



calculated. The first is based on the root mean square deviation (RMSD) definition, commonly used with impedance-based SHM practices. This damage metric is defined as follows:

$$RMSD = \frac{1}{n} \sqrt{\sum \frac{(Z_D - Z_{BL})^2}{Z_{BL}^2}}, \quad (3)$$

Where  $Z_D$  is the real component of the impedance signature of the part being tested,  $Z_{BL}$  is the real component of the baseline impedance signature and  $n$  is the total number of data points in the impedance signature.

The second damage metric used in this study is based on the correlation coefficient and is defined according to the following equation:

$$r = 1 - \left| \frac{n \sum Z_D Z_{BL} - \sum Z_D \sum Z_{BL}}{\sqrt{[n \sum Z_D^2 - (\sum Z_D)^2] [n \sum Z_{BL}^2 - (\sum Z_{BL})^2]}} \right|, \quad (4)$$

Where  $Z_D$ ,  $Z_{BL}$  and  $n$  follow the same definitions for equation (3). Following this definition, the value of this damage metric ranges from zero, when the two signatures are matching perfectly, and one, when there is no correlation between the current measurement and the baseline signature.

## 4. Results and discussion

In this section, the impedance signatures of all test specimens are presented and analyzed. For each set of test specimens, a baseline is first calculated by averaging the control parts' signature. These baselines provide a reference to which impedance signatures of the defected parts are compared. Defects are classified into three categories: dimensional inaccuracy, positional inaccuracy and internal porosity, as discussed in Section 3.1. The effectiveness of the proposed technique in detecting each of these defect types is then evaluated.

### 4.1 Establishing a baseline measurement

As described in Section 3.3, a baseline signature is first established by measuring and averaging the electromechanical impedance signatures of the two defect-free control parts in each test set. Figure 6 shows the real component of the impedance signatures of the control parts along with the averaged response for the VeroWhitePlus trussed specimens [Figure 6(a)], the nylon trussed specimens [Figure 6(b)] and the VeroWhitePlus impeller specimens [Figure 6(c)].

As discussed earlier, impedance signatures are measured over the frequency range of 4-9 and 4-20 kHz for the extruded nylon parts and the jetted VeroWhitePlus parts, respectively. These frequency ranges were selected such that the discrepancy between the impedance signatures of the control parts in each set is minimized. At the selected frequency ranges, it is noticed that control parts' impedance signatures accord very well; however, imperfections in the piezoelectric bonding process result in minor discrepancies. Such discrepancies are used later to define the detection threshold.

In this study, it is only assumed that the control parts are all free of defects. This is based on measurements of the parts' mass and the dimensional accuracy of their accessible features.

Internal printing defects may be present in these parts, which, in turn, may have contributed to the discrepancies in their impedance signatures. In practice, it is important to first ensure that the control parts are in fact defect-free via a combination of additional NDE techniques (such as CT scan measurements) so that a more accurate baseline signature is obtained. This results in narrowing the uncertainty bounds, and hence decreasing the detection threshold, allowing for smaller printing defects to be detected.

### 4.2 Effects of dimensional inaccuracy

Dimensional inaccuracies are represented by changes in the overall part mass due to printer malfunction and/or incorrect process parameters, as discussed in Section 3.1. In this study, parts featuring 1 and 5 per cent increase in mass were designed and fabricated to simulate this build error for both the extrusion and the jetting processes.

For specimens in Test Sets 1 and 2 (the trussed structures), mass increase was applied to the center pillar [Figure 4(a)]. For impeller specimens, on the other hand, mass increase was applied to the fins base [Figure 4(b)]. These errors were successfully detected by the proposed impedance-based NDE technique, as seen by comparing the measured impedance signatures with the corresponding baselines, as shown in Figure 7.

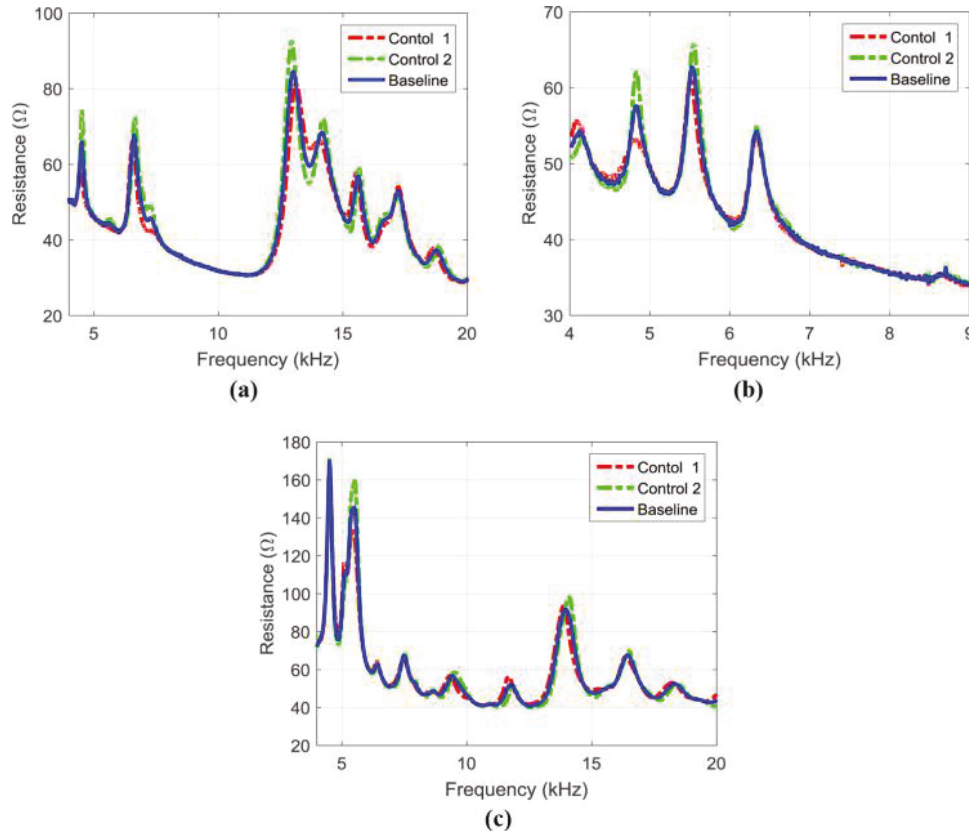
It has been reported that the frequency of impedance signature peaks can be correlated to the resonance frequencies of the test specimen. Hence, it is expected for a mass increase to result in a left-shift in impedance peaks. However, Figure 7(a)-(e) show an opposite trend, i.e. the peaks of the impedance signature shift to the right as more mass is added to the parts, indicating an increase in the overall stiffness of the structure. This suggests that the resulting increase in stiffness because of center pillar or fins base widening has more significant impact on part's dynamics than the accompanying increase in mass. As more mass is added, the shift in impedance peaks is found to increase, as can be seen in Figure 7(b) and (d). This is true for parts made by both extrusion and material jetting AM processes. In general, changes in stiffness because of dimensional inaccuracy depend on defect location, i.e. the place where the mass is added to the part. Hence, the trends reported in here may change depending on test specimens' geometry and defects' location.

### 4.3 Effects of positional inaccuracy

As indicated in Section 3.1, positional inaccuracy build defects, in which part mass remains equivalent to the control part but its location is different, are simulated by shifting certain features in test specimens. Specifically, a 1 mm diagonal shift of the center pillar of a part in Test Set 1, a warp in the upper surface of a part in Test Set 2 and a 20-degree offset of fins starting location in parts in Test Sets 3 are introduced to assess the ability of impedance-based NDE to detect this build defect. Impedance signatures of these parts are shown in Figure 8. The corresponding baseline signatures are also included to aid the comparison.

As can be observed, pillar displacement and warp defects are found to introduce a significant change in the impedance signature over the selected frequency ranges.

**Figure 6** Real component of the impedance signatures of the defect-free (control) parts, along with the baseline signature for (a) Test Set 1; (b) Test Set 2; and (c) Test Set 3



Fins offset defect, on the other hand, has a less significant, yet detectable, impact on the measured impedance signature. In general, the geometry of the part being tested, the location of the defect, its severity and the frequency range over which the part is being interrogated will determine the impact of the build defect on the measured impedance signature. To highlight the importance of frequency range selection on defects' detectability, the impedance signature of Test Set 3 control parts along with those corresponding to fins offset defect are measured over the 20- to 35-kHz frequency range. The results are presented in Figure 9. At this frequency range, the effect of the fins offset defect on the impedance signature is more profound compared to the 4- to 20-kHz range [Figure 8(c)], suggesting enhanced sensitivity. However, the variations among impedance signatures corresponding to the defect-free parts are more significant at higher frequencies (Figure 9). This expands the uncertainty bounds of the baseline measurement which adversely affects detection threshold and increases the possibility of false negatives.

The greater uncertainty in high-frequency baseline measurements can be mainly ascribed to the inconsistencies associated with the piezoelectric transducers' bonding process. Unknown defects in the assumed defect-free parts can also be an additional source of uncertainty. Eliminating these sources of uncertainty allows the utilization of higher frequency ranges for NDE. This will significantly improve the technique's

sensitivity, enabling the detection of minor printing defects. More consistent solutions for bonding piezoelectric transducers to test specimens, including instrumented testbeds and in-situ measurements, are currently being investigated by the authors.

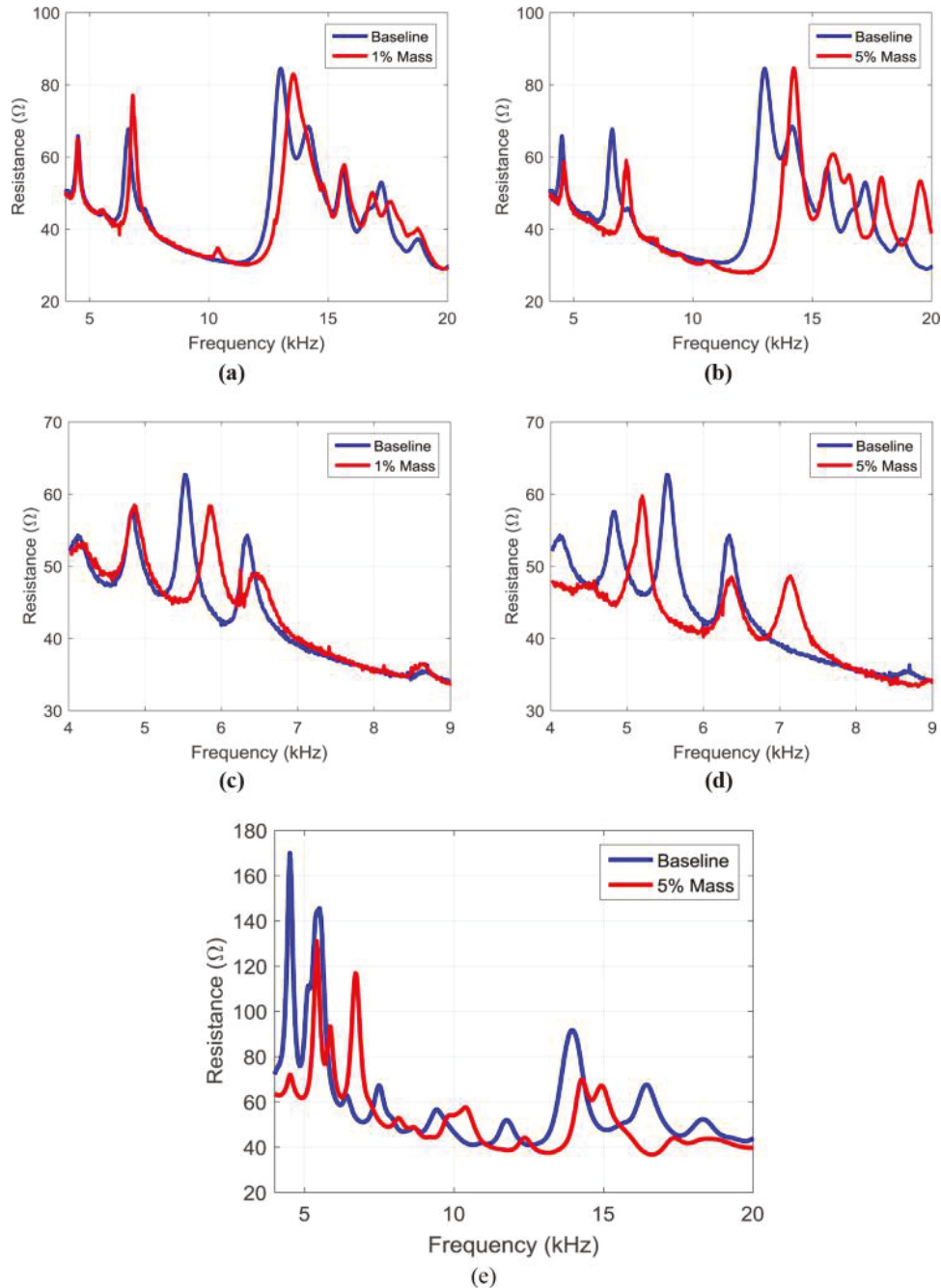
#### 4.4 Effects of internal porosity

To investigate the capability of impedance-based NDE to detect internal porosity, six test specimens featuring this build defect were designed and printed [Section 3.1; Figure 4(e)-(f)]. These specimens are distributed among the three test sets as follows:

- 1 *Test Set 1:* Three specimens with a 1-mm<sup>3</sup> void in the center pillar, an 8-mm<sup>3</sup> void in the center pillar and an 8-mm<sup>3</sup> void in the far corner pillar.
- 2 *Test Set 2:* One specimen with a 27-mm<sup>3</sup> void in the center pillar.
- 3 *Test Set 3:* Two specimens with hollow center pillars; the hollow section is 1 cm<sup>3</sup> in volume.

Impedance signatures for all six specimens are presented in Figure 10 along with the corresponding test set baseline signature.

In general, the impedance signatures of the void defects, except for Test Set 3 specimens, can hardly be distinguished from the baseline signature. This is especially true for the case of the 8-mm<sup>3</sup> void in the center and far corner pillars of Test Set 1 specimens [Figure 10(b) and

**Figure 7** Impedance signatures of the parts with dimensional inaccuracies as compared to the baseline signature

**Notes:** (a) 1 per cent and (b) 5 per cent mass increase by widening the center pillar of parts of Test Set 1; (c) 1 per cent ; (d) 5 per cent mass increase by widening the center pillar of parts of Test Set 2; (e) 5 per cent mass increase by widening the base of the fins of parts of Test Set 3

(c). It is noticed that Test Set 1 specimen with the 1-mm<sup>3</sup> void in the center pillar [Figure 10(a)] shows a more significant deviation from the baseline signature as compared to the larger void in the same location [Figure 10(b)]; however, this is attributed to a small defect on the part's edge that occurred during post-processing. One potential cause for such small deviations in impedance signatures corresponding to these defects is the presence of

support material within the voids. This support material causes the total mass of the part to remain nearly the same, and thus blurs voids' effects on the overall dynamic response. Furthermore, the frequency range over which impedance signatures are measured seems to be very low to detect voids of such size.

For Test Set 2 specimen, a larger void size was introduced so as to make it distinguishable from the natural

**Figure 8** Impedance signatures for (a) a Test Set 1 specimen with a 1 mm displacement of the center pillar; (b) a Test Set 2 specimen with warp on the upper face; and (c) a Test Set 3 specimen with fins offset

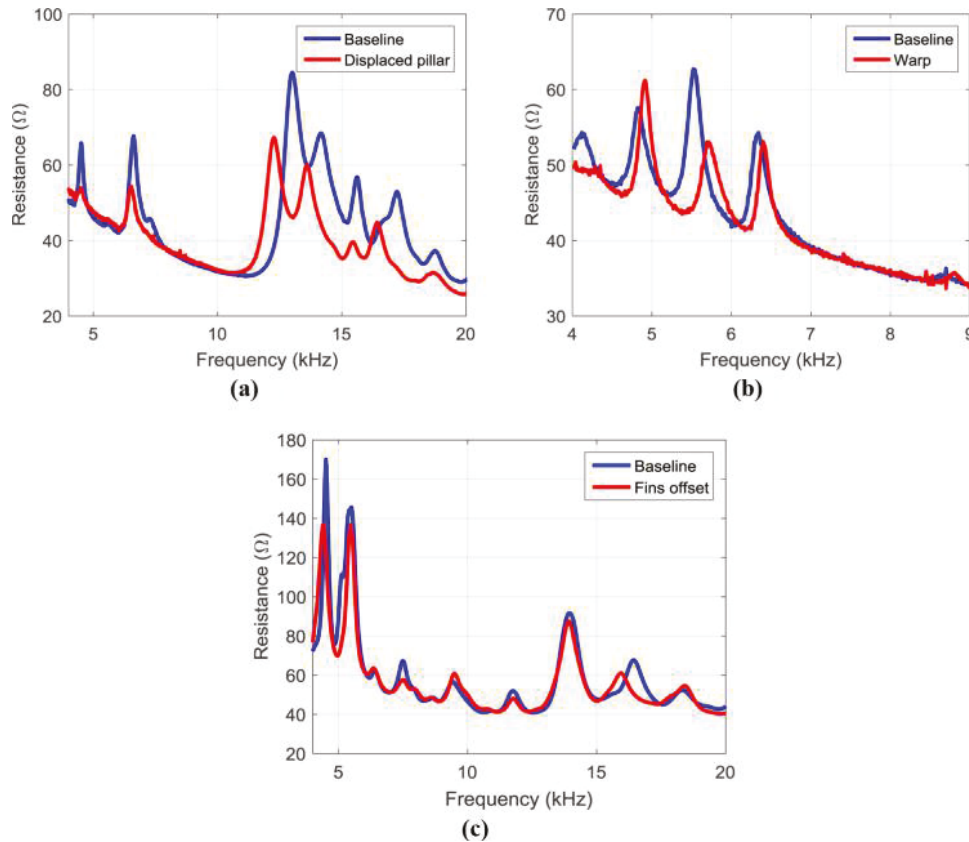
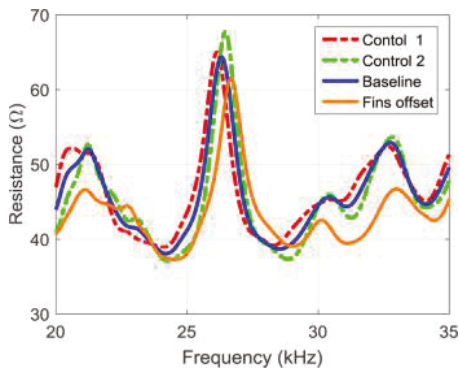


**Figure 9** Baseline signature for Test Set 3 along with the impedance signatures of individual control parts and that featuring positional inaccuracy build defect

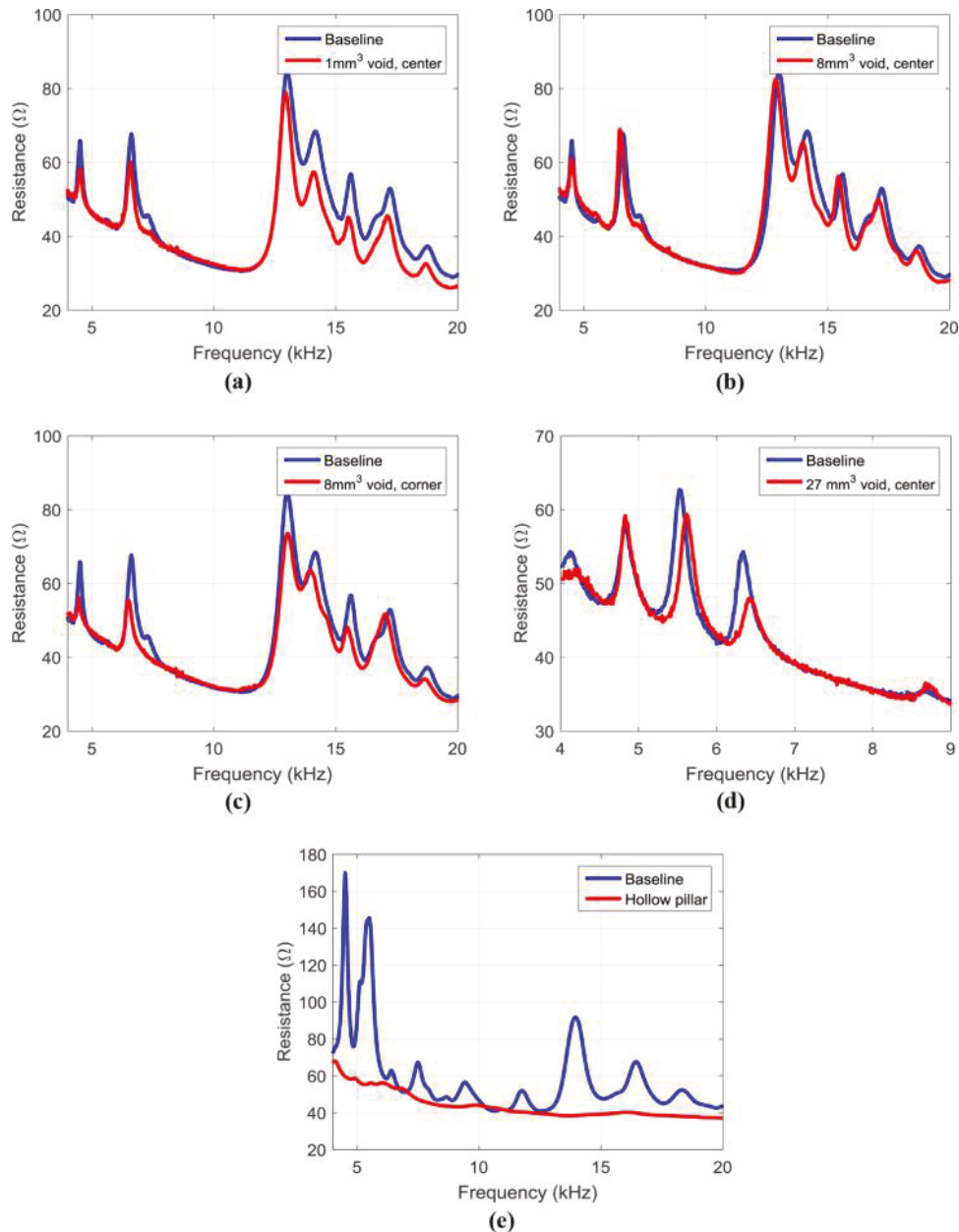


porosity associated with extrusion processes. Unlike material jetting, where fully dense parts are normally obtained, extrusion process leaves small gaps between material lines. Thus, extremely small voids are likely to be indistinguishable from those naturally occurring in the process. It is worth noting that because of its size, the void is self-supporting and is not filled with support material as it is the case for other specimens. Examining the impedance signature for this specimen, [Figure 10(d)] shows that this defect is clearly distinguishable from the baseline signature.

Moreover, the right shift in impedance peaks indicates that for the selected frequency range, the effect of inertia reduction, as a result of the void being completely empty, is more significant than the accompanying stiffness reduction.

The impeller specimens with the hollow center pillar represent an extreme example of internal porosity defects. The hollow section is about 17 per cent of the total volume of the part, and it is completely filled with support material. This extremely large void results in a drastic change in the impedance signature [Figure 10(e)]. Furthermore, the large amount of support material in the hollow section increases damping significantly, which results in suppressing most of the peaks in the impedance signature, as seen in the figure.

Unlike dimensional and positional inaccuracies build defects, internal porosity defects seem to have a smaller impact on the dynamic response of the test specimens, especially at low frequencies. Further investigations are needed to address the effects of internal porosity build defects on impedance signatures, and the range of void sizes that can be detected with the proposed impedance-based NDE. This is expected to be dependent on the frequency range over which the test specimen is interrogated, the material and AM process used to fabricate the specimen and the location of the void. The noticeable increase in damping, due to the presence of support material, can also be utilized to detect the presence of internal voids.

**Figure 10** Impedance signatures for the parts featuring internal porosity

**Notes:** Test Set 1 specimens with (a) a 1-mm<sup>3</sup> void in the center pillar; (b) an 8-mm<sup>3</sup> void in the center pillar; (c) an 8-mm<sup>3</sup> void in the far corner pillar; (d) Test Set 2 specimen with a 27-mm<sup>3</sup> void in the center pillar; (e) Test Set 3 specimen with a hollow center pillar

#### 4.5 Analysis of results

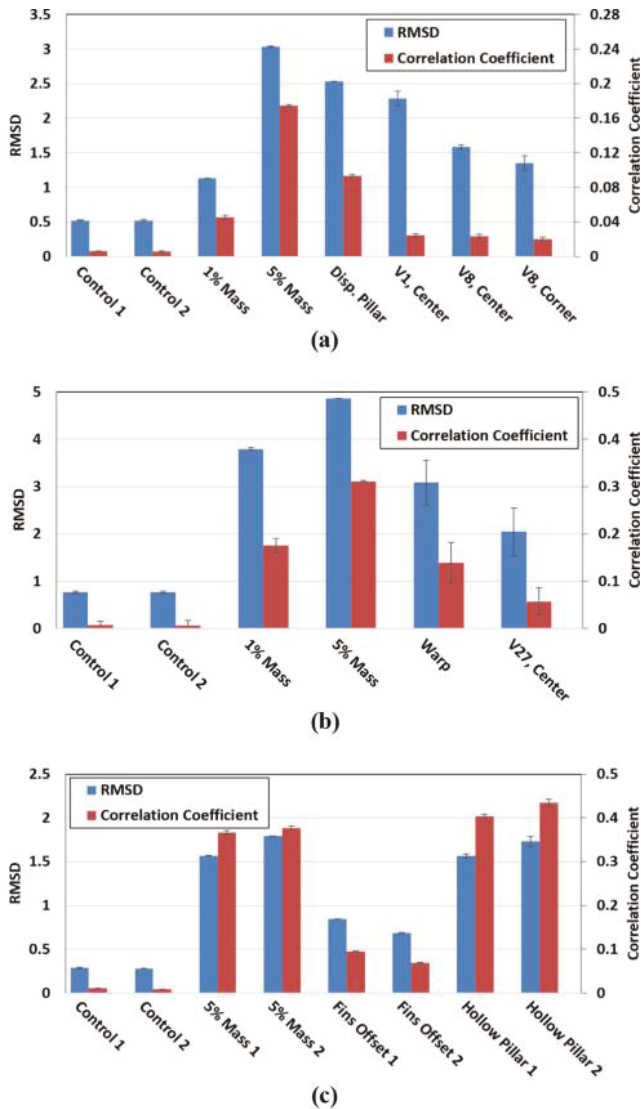
Two damage metric definitions (root mean square deviation and correlation coefficient defined in Section 3.3) are adopted in this study to quantify the variations in the impedance signature induced by various build defects. Following these definitions, damage metrics for specimens in all three test sets are calculated, the results are depicted in Figure 11.

Damage metric values for dimensional inaccuracy and positional inaccuracy build defects are found to be considerably larger than those for the defect-free parts (Control 1 and Control 2). Thus, it can be concluded that a

simple analysis of impedance signatures is sufficient to detect these two build defects with high confidence. This is true for specimens made by both material jetting and extrusion processes.

Internal porosity defects, on the other hand, are found to result in a much smaller damage metric values, except for the extreme case of the completely hollow center pillar in Test Set 3. Therefore, it is possible for such defects to be left undetected, resulting in false negatives. However, this may be mitigated by interrogating the structure at higher-frequency ranges, provided that baseline signature can be determined

**Figure 11** Damage metrics values for (a) Test Set 1; (b) Test Set 2; and (c) Test Set 3



**Notes:** In the figure, V1, V8 and V27 denote respectively specimens with 1-, 8- and 27-mm<sup>3</sup> void sizes at specified locations

with high certainty (as discussed in Section 4.3). Furthermore, the added damping due to the presence of the support material in the voids can be utilized to detect this type of build defects.

Although damage metric values for the control parts should ideally be zero, variations introduced by the piezoelectric transducers' bonding process along with noise contamination result in greater than zero damage metric values, as shown in Figure 11. This provides a quantitative measure of the uncertainty in the baseline measurement. This also provides a lower bound for the damage detection threshold. This means that a specimen with a damage metric value greater than this threshold will be flagged as defective. A tight damage detection threshold increases the probability of capturing defective parts at the cost of having more false positives and vice versa. Overall cost along with the mission the part is

serving need to be taken into consideration when setting the value of the damage detection threshold.

These results suggest that the proposed impedance-based technique provides a promising solution for NDE and QC of AM parts. The technique is capable of detecting several types of build defects commonly encountered in AM. Additional work is needed to further investigate the capabilities of this technique, define the sensitivity margins to different types of structural defects and identify optimal frequency ranges for different materials and processes. It is expected that the sensitivity of the proposed technique will enhance when stiffer, lightly damped materials, such as metals, are tested, as suggested by the existing literature on SHM of metallic and nonmetallic structures (Wang and Zou, 2013; Annamdas and Radhika, 2013; Zagrai *et al.*, 2010). In their future work, the authors will systematically test AM metallic parts to study the effects of their superior properties on the technique's performance and capabilities.

## 5. Conclusions

The lack of suitable NDE techniques for qualifying and certifying end-use products fabricated via AM is seen as a major barrier to the further industrial adoption of AM technologies. Thus, there are several calls for novel NDE techniques that are suitable for accurate inspection of AM parts with complex geometry (e.g. inaccessible features, internal channels, etc.), rough surfaces and deeply embedded flaws. To address this research gap, the authors propose an NDE technique that uses electromechanical impedance measurements to indirectly measure printed part abnormalities.

To evaluate the feasibility of this technique, the authors first designed and fabricated a suite of test specimens with representative defects of AM processes, including dimensional inaccuracies, positional inaccuracies and internal porosities. An impedance-based analysis was conducted on each defective specimen and then compared to a baseline measurement of a defect-free part. Through this analysis, it was determined that the technique is a feasible means of detecting defects in AM parts. Specifically, it was shown that the technique is capable of detecting print defects, resulting in mass change (as small as 1 per cent) and in feature displacement (as small as 1mm) in both extruded nylon parts and jetted VeroWhitePlus parts. Internal porosity defects were also detectable; however, damage metric values associated with this defect type were relatively small, which can lead to false negatives.

While the feasibility of the approach has been demonstrated, there remain several opportunities for future research. The authors look ahead to quantifying the sensitivity of the approach relative to defect type, size and location. Assessing the effects of parts size and material on the techniques performance is another area of research. The authors also look to conduct additional tests on directly printed metal parts to study the effects of their superior stiffness on the technique's sensitivity.

In this paper, impedance-based NDE is proposed as a post-process NDE approach that would allow for simple detection of print defects via a go/no-go decision based on the evaluated damage metrics. In future work, the authors look to

expand the application of this technique as a means of detecting, locating and quantifying part defects through in-depth analysis of impedance signatures coupled with machine learning algorithms and dynamic modeling.

## References

- Albakri, M.I. and Tarazaga, P.A. (2016), “Electromechanical impedance based damage characterization using spectral element method” *Journal of Intelligent Materials Systems and Structures*, Vol. 28 No. 1, doi: 10.1177/1045389X16648426.
- Albakri, M.I., Sturm, L.D., Williams, C.B. and Tarazaga, P.A. (2015), “Non-destructive evaluation of additively manufactured parts via impedance-based monitoring”, International Solid Freeform Fabrication Symposium, Austin, TX, 10-12 August.
- Annamdas, V.G. and Radhika, M.A. (2013), “Electromechanical impedance of piezoelectric transducers for monitoring metallic and non-metallic structures: A review of wired, wireless and energy-harvesting methods”, *Journal of Intelligent Materials Systems and Structures*, Vol. 24 No. 9, pp. 1021-1042.
- Annamdas, V.G.M. and Soh, C.K. (2010), “Application of electromechanical impedance technique for engineering structures: review and future issues”, *Journal of Intelligent Materials Systems and Structures*, Vol. 21 No. 1, pp. 41-59.
- ASTM (2017), *Committee F42 on Additive Manufacturing Technologies*, available at: [www.astm.org/COMMITTEE/F42.htm](http://www.astm.org/COMMITTEE/F42.htm)
- GE Aviation (2014), “Fit to print: new plant will assemble world’s first passenger jet engine with 3D printed fuel nozzles, next-gen materials”, GE Reports, 23 June, available at: [www.gereports.com/post/80701924024/fit-to-print](http://www.gereports.com/post/80701924024/fit-to-print)
- Giurgiutiu, V. and Zagrai, A.N. (2000), “Characterization of piezoelectric wafer active sensors”, *Journal of Intelligent Materials Systems and Structures*, Vol. 11 No. 12, pp. 959-976.
- Leo, D.J. (2007), *Engineering Analysis of Smart Material Systems*, Wiley, Hoboken, NJ.
- Liang, C., Sun, F.P. and Rogers, C.A. (1994), “Coupled electro-mechanical analysis of adaptive material systems – Determination of the actuator power consumption and system energy transfer”, *Journal of Intelligent Materials Systems and Structures*, Vol. 5 No. 1, pp. 12-20.
- NIST (2013), *Measurement Science Roadmap for Metal-based Additive Manufacturing*, Energetics, available at: [www.nist.gov/el/isd/upload/NISTAdd\\_Mfg\\_Report\\_FINAL-2.pdf](http://www.nist.gov/el/isd/upload/NISTAdd_Mfg_Report_FINAL-2.pdf)
- Nokes, J.P. and Cloud, G.L. (1993), “The application of interferometric techniques to the nondestructive inspection of fiber-reinforced materials”, *Experimental Mechanics*, Vol. 33 No. 4, pp. 314-319.
- Park, G., Cudney, H. and Inman, D.J. (2000a), “An integrated health monitoring technique using structural impedance sensors”, *Journal of Intelligent Materials Systems and Structures*, Vol. 11 No. 6, pp. 448-455.
- Park, G., Cudney, H. and Inman, D. (2000b), “Impedance-based health monitoring of civil structural components”, *Journal of Infrastructure Systems*, Vol. 6 No. 4, pp. 153-160.
- Park, G., Sohn, H., Farrar, C.R. and Inman, D.J. (2003), “Overview of piezoelectric impedance-based health monitoring and path forward”, *Shock Vibration Dig*, Vol. 35 No. 6, pp. 451-464.
- Pears, D.M., Tarazaga, P.A. and Inman, D.J. (2007), “Frequency range selection for impedance-based structural health monitoring”, *Journal of Vibration and Acoustics*, Vol. 129 No. 6, p. 701.
- Plessis, A., Roux, S., Els, J., Booysen, G. and Blaine, D. (2015), “Application of microCT to the non-destructive testing of an additive manufactured titanium component”, *Case Studies in Nondestructive Testing and Evaluation*, Vol. 4, pp. 1-7.
- SpaceX (2014), “SpaceX launches 3D-printed Parto Space, creates printed engine chamber”, 31 July, available at: [www.spacex.com/news/2014/07/31/spacex-launches-3d-printed-part-space-creates-printed-engine-chamber-crewed](http://www.spacex.com/news/2014/07/31/spacex-launches-3d-printed-part-space-creates-printed-engine-chamber-crewed)
- Stratasys (2015), “Additive manufacturing for aerospace: FAA-approved air duct for ‘flying eye hospital’ produced in just days”, available at: <http://blog.stratasys.com/2015/03/05/3d-printed-air-duct-flying-eye-hospital>
- Sturm, L.D., Williams, C.B., Camelio, J., White, J. and Parker, R. (2014), “Cyber-physical vulnerabilities in additive manufacturing systems”, International Solid Freeform Fabrication Symposium, Austin, TX, 4-6 August.
- Waller, J., Parker, B.H., Hodges, K.L., Burke, E.R. and Walker, J.L. (2014), *Nondestructive Evaluation of Additive Manufacturing: State-of-the-Discipline Report*, NASA/TM-2014-218560.
- Wang, H. and Zou, L. (2013), “Interfacial effect on the electromechanical behaviors of piezoelectric/elastic composite smart beams”, *Journal of Intelligent Materials Systems and Structures*, Vol. 24 No. 4, pp. 421-430.
- Zagrai, A., Doyle, D., Gigineishvili, V., Brown, J., Gardenier, H. and Arritt, B. (2010), “Piezoelectric wafer active sensor structural health monitoring of space structures”, *Journal of Intelligent Materials Systems and Structures*, Vol. 21 No. 9, pp. 921-940.

## Corresponding author

**Mohammad I. Albakri** can be contacted at: [malbakri@vt.edu](mailto:malbakri@vt.edu)